Au-GaAs(110) interface: Photoemission studies of the effects of temperature

W. G. Petro,* T. Kendelewicz, I. Lindau, and W. E. Spicer
Stanford Electronics Laboratories, Stanford University, Stanford, California 94305
(Received 1 October 1985; revised manuscript received 21 July 1986)

Detailed photoemission studies have been performed on the Au-GaAs(110) interface at room temperature and after annealing at temperatures of up to 500 °C. The data indicate the formation of a Au-rich Au-Ga alloy in the form of medium-to-large-scale (bulklike) clusters with possible As intermixing at room temperature. The degree of intermixing increases with annealing temperature, as the clusters become thicker and more enriched in Ga. At 500 °C the As evaporates, large portions of the GaAs surface become uncovered, and evidence of a nearly pure metallic Ga phase is seen. The Fermi-level pinning behavior has also been deduced from the photoemission data. We observe pinning at a barrier height of 0.7 ± 0.1 eV below the conduction-band minimum (CBM) for small [~0.2 monolayer (ML)] coverages and at 0.85 ± 0.1 eV below the CBM for coverages greater than ~0.3 ML on n-type GaAs(110) at room temperature. We suggest that the pinning at 0.7 eV is due to an acceptor defect level and the pinning at 0.85 eV is due to a donor defect level which, due to depletion of electrons from the defect level by the Au clusters, acts effectively to pin E_F on n-type GaAs. These levels are in agreement with those of the unified defect model. After heating of these films we observe a reduction in the amount of pinning due to annealing of defects and exposure of large portions of the surface. Pinning on p-type GaAs is observed at 0.5 ± 0.1 eV above the valence-band maximum for a coverage of ~0.2 ML at room temperature and is attributed to the same donor level. This pinning is also seen to decrease with increased annealing temperature.

I. INTRODUCTION

An understanding of the interactions between metal overlayers and compound semiconductor surfaces is basic to the fabrication of electronic devices, which utilize metal contacts to form active Schottky barriers as well as ohmic contacts. Most contacts to semiconductor devices are subjected to various heat treatments during processing;[1] one reason for this is to promote firm metal adhesion to the semiconductor.[2] Recent developments in self-aligned gate technology, which uses the metal overlayer as a mask for ion implantation, require annealing at temperatures of 800–850 °C.[3,4] The effects of annealing on Au-GaAs devices are important not only as a necessary processing step but also as a result of the often high temperatures (~200 °C) achieved during device operation. These high temperatures lead to premature failure as a result of Au or a Au-rich alloy penetrating the active device layer.[5–7] Such interdiffusion has been observed to cause a decrease in the apparent Schottky-barrier height on n-type GaAs from ~0.9 V to ~0.6 V, while at the same time causing an increase in the ideality factor from ~1.0 to ~1.2.[8,9] These values are based on I-V and C-V electrical measurements, and as such are dependent upon the particular model of the conduction mechanism used to interpret the data. Madams *et al.*[10] have used a thermionic field emission model to conclude that the barrier height remains unchanged at ~0.95 V after heating to 450 °C and that the Ga outmigration results in the formation of an n^+ region beneath the contact.

Only during the past few years have systematic attempts been made to understand the effects of chemistry on the electrical properties of the interface. Details of this work may be found in the papers of Lindau *et al.*,[11] Spicer *et al.*,[12] Brillson,[13] and references therein. Intermixing during the formation of Au-GaAs contacts at room temperature on the cleaved GaAs(110) surface has been demonstrated in earlier work.[14,15] It was established that both Ga and As move through the Au overlayer, even for thicknesses as great as ~200 Å. Studies of high-temperature annealing of Au-GaAs interfaces prepared on chemically cleaned GaAs(100) and (111) wafer surfaces have been made using a wide variety of experimental techniques. Rutherford backscattering measurements have demonstrated Ga outmigration to the surface[10,9,16] and deep Au diffusion into the GaAs.[17] Auger electron spectroscopy with Ar^+-ion sputter depth profiling has shown that Ga and much smaller amounts of As accumulate at the surface with no Ga or As present in the bulk of the film.[18,16] Other techniques have demonstrated similar behavior; these include scanning electron microscopy,[16,19,20] transmission electron microscopy,[21] secondary ion mass spectrometry,[22] He^+-ion scattering,[23] and x-ray diffractometry.[22] Studies using mass-spectrometer-evolved gas analysis[24,19] have shown directly that As is released during heating. Intermixing of Si and Au has also been reported on Au-Si structures.[25,26] In addition, studies have been made of Au alloy contacts to GaAs.[27–29]

In the present work we have performed detailed photoemission measurements of Au overlayers on GaAs(110) at room temperature (RT). We have studied core-level line shapes, binding-energy (E_B) shifts, and intensity variations to establish the nature of the chemical states resulting from surface interactions. We have also used the same techniques to investigate both the details of the in-

terdiffusion process and changes in the Schottky-barrier height with increasing annealing temperatures. We find that I-V and C-V measurements made on identically prepared and similarly processed thick-layer device structures[30,31] support the photoemission measurements and lead to a mechanism for explaining the observed behavior of the structures studied in this work as well as those studied in the earlier work mentioned above.

II. EXPERIMENTAL

A. Sample preparation

All of the GaAs(110) surfaces were prepared by cleavage *in situ* under ultrahigh vacuum[32] at a pressure of less than 1×10^{-10} Torr, exposing a square 5×5 mm^2 cleavage face. A Te-doped n-type ($n=8\times10^{17}$ cm^{-3}) single-crystal sample was used for the low- and high-coverage heating experiments and the room-temperature ultraviolet photoemission spectroscopy (UPS) experiments, and an undoped n-type ($N_D=1\times10^{17}$ cm^{-3}) single-crystal sample was used for the room-temperature soft x-ray photoemission spectroscopy (SXPS) experiments. A Zn-doped p-type ($p=2\times10^{18}$ cm^{-3}) single-crystal sample was used for room-temperature UPS and low-coverage heating experiments. Au was deposited from a bead on a tungsten filament; two quartz-crystal thickness monitors (one near the evaporator, which was used during the evaporation, and one which could be situated at the sample position) were used to calibrate and control the evaporation rate. Exposures were made by opening a shutter on the evaporator for times no greater than $\sim$40 sec in order to minimize heating of the sample due to radiation from the evaporator (measurements made by placing a thermocouple at the sample position indicated a temperature increase of less than 10 °C). The pressure during evaporations was less than 2×10^{-10} Torr. Au coverages were determined from the amount of Au incident on the sample surface assuming unity sticking coefficient with one monolayer (ML) defined to be one Au atom per surface Ga and As atom (1 ML$=8.85\times10^{14}$ atoms/cm^2). Using the bulk density of Au we find that 1 ML$=1.5$ Å.

In the heating experiments the sample was heated by a tungsten filament heater at the desired temperature for 10 to 15 min and then allowed to cool to room temperature before measurements were taken. The base pressure during sample heating was $\sim2\times10^{-10}$ Torr. All cleaves and evaporations were performed with the sample at room temperature.

B. Photoemission spectra

Photoemission energy distribution curves (EDC's) for room-temperature and low-coverage (0.2 ML) heating experiments on n- and p-type samples were obtained with a monochromatized He discharge lamp source[33,34] that provided photon energies of 21.2 eV for valence-band spectra and 40.8 eV for Ga $3d$ core-level spectra. Room-temperature and high-coverage (15 ML) heating data on n-type samples were obtained using synchrotron radiation from the I-1 4° beam line at the Stanford Synchrotron Radiation Laboratory (SSRL).[35] The room-temperature experiments at SSRL were performed during parasitic (low beam current) operation of the storage ring and the EDC intensities were normalized to a signal from a photon flux monitor mounted between the monochromator output port and the sample chamber. The high-coverage heating experiments were performed during dedicated (high beam current) operation and the EDC intensities were normalized to this beam current. These core-level and valence-band studies required photon energies in the region from 100 to 130 eV which were provided by a grazing-incidence grasshopper monochromator described by Brown *et al.*[36] Photoemitted electrons were energy analyzed using an angle-integrated double-pass cylindrical mirror analyzer (CMA) described by Pianetta *et al.*[32]

The resolution of the CMA was adjustable from 0.17 to 0.35 eV and the monochromator resolution ranged from 0.08 to 0.15 eV.[37] The reproducibility of the measurements allowed determination of relative core-level shifts to an accuracy of ±0.05 eV, while absolute values of core-level energies were accurate to within ±0.1 eV. The position of the surface Fermi level (E_{F_s}) was determined from the EDC of a thick (>100 Å) Au film evaporated *in situ* onto a stainless-steel substrate in electrical and thermal contact with the semiconductor samples. Movement of the semiconductor valence-band maximum (VBM) relative to E_{F_s} with increasing Au coverage or annealing temperature was determined from movement of the Ga and As $3d$ core levels and VBM edge relative to their values on the clean surface. In this way E_{F_s} could be located to within $\sim\pm0.1$ eV on the clean and covered surfaces. The escape depth of the photoemitted electrons was ~10 Å for the UPS experiments and ~5 Å for the SXPS experiments;[38] thus, effects of the escape depth on the band bending as measured by the core-level shifts are small compared to the experimental resolution.[39]

III. THE Au-GaAs INTERFACE AT ROOM TEMPERATURE

In this section we present and discuss in detail photoemission data for the Au-GaAs interface at room temperature. We find that the picture that emerges for the behavior at room temperature provides an excellent background for understanding the somewhat more complex effects of heating which are presented and discussed in Sec. IV.

A. Results

The photoemission data presented here were collected during two separate experiments. In the first experiment (UPS) we studied Au overlayers on n- and p-type GaAs(110) surface (see Sec. II A) using the He-discharge lamp with monochromator to obtain photon energies of 21.2 eV for the valence-band region and 40.8 eV for the Ga $3d$ core level. In the second experiment (SXPS) we studied the n-type GaAs(110) surface using synchrotron radiation to provide photon energies of 100 eV for the Ga $3d$ and As $3d$ core levels and 130 eV for the Au $4f$ core levels.

1. *Energy distribution curves*

a. The valence-band region. The valence-band spectra taken with $h\nu=21.2$ eV are shown in Fig. 1 for Au thicknesses from 1.1×10^{15} to 25×10^{15} atoms/cm^2 (1.2 to 28 ML) on n-type GaAs(110). The kinetic energies (measured in vacuum) of the photoemitted electrons range from 8 to 16 eV, corresponding to escape depths of ~5 to 10 Å; thus, very little emission from the substrate valence band is to be expected above 14×10^{15} atoms/cm^2 (~24 Å) for uniform Au coverage. As seen in Fig. 1 the spectrum in this coverage range is dominated by the Au $5d$ bands and sp emission up to the Fermi edge. The two strong peaks appear at -6.2 and -4.3 eV, with a low-binding-energy shoulder on the -4.3-eV peak.

b. The Ga 3d core level. The Ga $3d$ core-level peak for both n- and p-type surfaces was monitored using a photon energy of 40.8 eV. This results in a kinetic energy of ~17 eV in vacuum, at which the background due to inelastically scattered secondary electrons becomes large, particularly at the higher Au coverages. Thus a higher photon energy is required in order to observe any small changes in the shape of the Ga $3d$ core level. Such data taken at a photon energy of 100 eV are shown in Fig. 2. The large initial shift of the core level to higher kinetic energy is due to band bending, as the VBM moves closer to the Fermi level for the n-type surface. Additional shifting of the core level toward higher kinetic energy can be seen as the Au coverage is increased. Details of this movement are presented graphically in Fig. 8 in Sec. III A 2 *b*. Comparison of the peak shapes for each coverage shows a de-

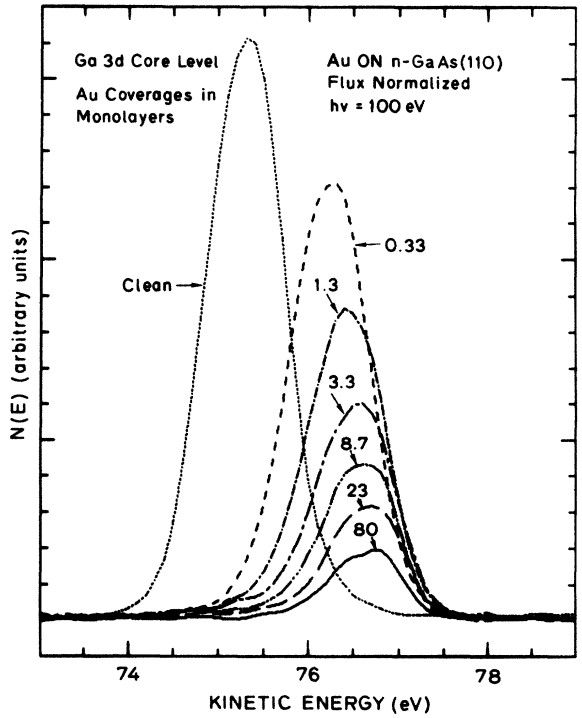

FIG. 2. Photoemission energy distribution curves of the Ga $3d$ core level taken at a photon energy of 100 eV for increasing Au overlayer thicknesses. Each spectrum is normalized to the incident photon flux.

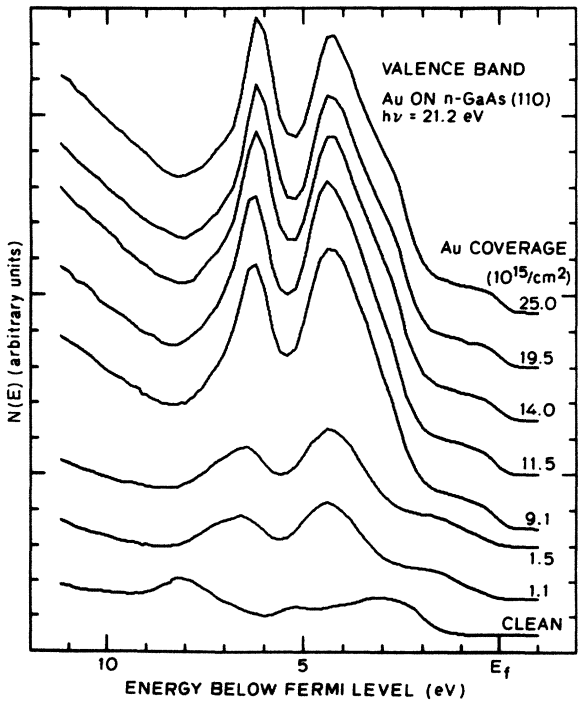

FIG. 1. Photoemission energy distribution curves of the valence-band region taken at a photon energy of 21.2 eV for increasing Au overlayer thicknesses on n-type GaAs(110).

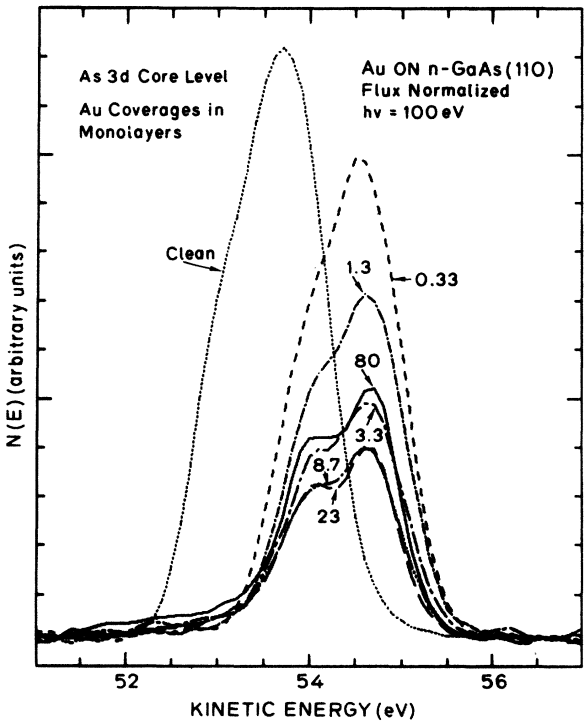

FIG. 3. Photoemission energy distribution curves of the As $3d$ core level taken with a photon energy of 100 eV for increasing Au overlayer thicknesses. Each spectrum is normalized to the incident photon flux.

crease in the full width at half maximum (FWHM) of ~ 0.1 eV for the 80-ML peak relative to the clean peak. The peaks also exhibit a tail on the high-binding-energy side that increases with Au coverage.

c. The As 3d core level. The As $3d$ core-level spectra, shown in Fig. 3, were taken at the same photon energy as the Ga $3d$ core levels. This allows both spectra to be taken during the same energy scan of the CMA so that the relative intensity ratios can be accurately compared from one coverage to the next. The As $3d$ core level shows an initial band-bending shift close to that of the Ga $3d$ one, then remains relatively fixed in energy (see Sec. III A 1 *b*). Close comparison of the core-level shapes shows a high-binding-energy tail similar to that of the Ga $3d$ core level.

d. The Au 4f core levels. The Au $4f$ core-level spectra, shown in Fig. 4, were taken with a photon energy of 130 eV. The upper curve shows the spectrum taken from a thick (~ 200 Å) Au film evaporated *in situ* onto a stainless-steel substrate in electrical contact with the sample (the same film was used to locate E_F). The peak intensities increase monotonically with increasing Au coverage, and both the $4f_{5/2}$ and $4f_{7/2}$ components move continuously toward lower binding energy, approaching that of pure bulk Au. A total shift of 0.37 eV was measured as the Au coverage was increased from 0.33 to 80 ML. There was no measurable change in the splitting of the two spin-orbit components with increasing Au coverage.

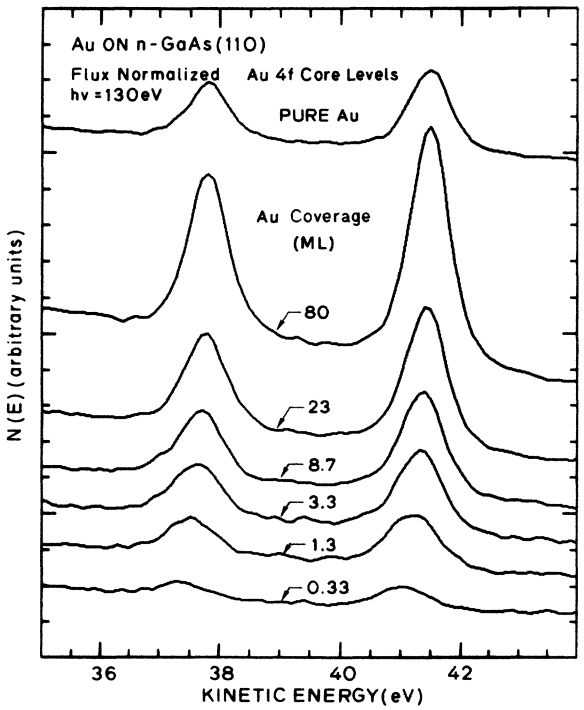

FIG. 4. Photoemission energy distribution curves of the Au $4f$ core levels taken with a photon energy of 130 eV and normalized to the incident photon flux for increasing Au coverages. The upper curve is the spectrum for a pure Au film evaporated *in situ* onto a stainless-steel substrate.

2. Results derived from EDC's

a. Peak shapes and intensities. Changes in the linewidths of the core-level peaks can be important in determining the presence of "chemically" shifted peaks, in addition to the main substrate peak, which are often too close in energy to be clearly resolved. The implications of the linewidth changes described here are discussed in Sec. III B 1. As described previously in Sec. III A 1 *b*, the width of the Ga $3d$ peak is observed to narrow monotonically as the Au coverage is increased from zero to 80 ML. A more complex behavior can be observed in the As $3d$ line shape, the details of which are shown in Fig. 5. The FWHM decreases sharply after the first Au deposition of 0.33 ML, then gradually increases as the coverage is increased to about 10 ML. The width then narrows again as the coverage is increased from 10 to 80 ML. The Au $4f$'s show a monotonic decrease in linewidth (similar to that of the Ga $3d$) as the Au coverage is increased.

The development of the intensities of the Ga $3d$, As $3d$, and Au $4f$ peaks as a function of Au coverage is shown in Fig. 6. The data points were determined from the total areas under the As $3d$, Ga $3d$, and Au $4f_{5/2}$ plus $4f_{7/2}$ peaks at each Au coverage. Each point is normalized to the area under the peak for the clean surface in the case of Ga and As (left-hand scale) and to the area under the lowest coverage (0.33 ML) peaks in the case of Au (right-hand scale). The exponential curve is the expected result for an abrupt, uniform Au overlayer, assuming a scattering length $L(E)$ of 5 Å and an angle ϕ of 42.6° (the CMA collection angle) between the sample surface normal and the direction of the photoemitted electrons. The exponential attenuation is then given by

$$I(\theta)/I(\text{clean}) = \exp\{-t\theta/[L(E)\cos\phi]\} ,$$

where θ is in ML, $L(E)$ is in Å, and $t = 1.5$ Å/ML is the thickness of 1 ML of Au as determined from the bulk Au density.

It is evident that initially the As $3d$ and Ga $3d$ intensities decrease at the same rate and closely follow the exponential curve. For coverages above ~ 3 ML, however, the [As/Ga] ratio increases monotonically. The ratio $I(\theta)/I(\text{clean})$ for As reaches a minimum at 8.7 ML and then increases at the higher coverages. The corresponding

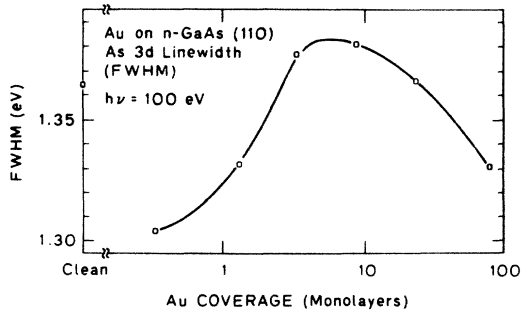

FIG. 5. Plot of the linewidth (FWHM) of the As $3d$ core level taken at a photon energy of 100 eV as a function of Au coverage on *n*-type GaAs(110).

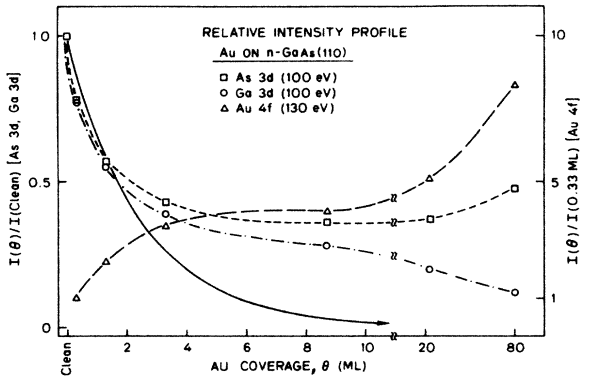

FIG. 6. Relative intensity profiles—$I(\theta)/I$(clean) for the Ga $3d$ and As $3d$ core levels and $I(\theta)/I$(0.33 ML), axis on the right, for the Au $4f$ core levels—as a function of average Au coverage θ in ML for n-type GaAs(110). The solid curve represents the exponential decay of the Ga $3d$ and As $3d$ core-level intensities expected for uniform growth of an abrupt Au overlayer.

ratio for Ga continues to decrease for these coverages. The ratio $I(\theta)/I$(0.33 ML) for the total Au $4f_{5/2,7/2}$ peaks increases continuously with increasing coverage, with a plateau for $6<\theta<10$ ML.

b. Binding-energy shifts and Fermi-level pinning. The binding energies of the Ga $3d$, As $3d$, and Au $4f$ and $5d$ core levels as a function of increasing Au coverage can be of much use in identifying the chemical nature of the bonds produced at the interface. The measured Au $4f_{7/2}$ binding energy relative to E_F is shown in Fig. 7. This measured value can be compared directly with the binding energies of the Au $4f$'s in various Au-Ga alloys or Au clusters[40–42] as long as the clusters are large enough to define a Fermi level, since charge in the metal can move to screen the band-bending charge in the semiconductor.[43] For very low coverages (where the metal becomes atomic-like) this screening may not be complete. The effects of band bending have often been accounted for when determining semiconductor-core-level-to-VBM binding energies and even metal-overlayer-core-level-to-VBM energies for low metal coverages.[44] However, given the existence of a metallic Fermi edge for the metal overlayer in equilibrium with the substrate, we assume that the band-bending charge is fully screened.

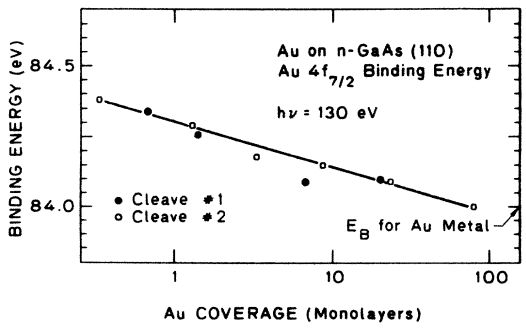

FIG. 7. Au $4f_{7/2}$ binding energy relative to the Fermi level as a function of Au coverage on n-type GaAs(110).

The energy shifts of the Ga $3d$ and As $3d$ core levels are plotted in Fig. 8. For n-type surfaces the position of the maximum of the low-binding-energy component of the $3d_{3/2,5/2}$ core-level peak was taken to be the $3d_{5/2}$ position. The position of the Fermi level on the clean cleaved surface was 1.43 eV above the valence-band maximum. Thus the quantity plotted along the vertical axis is given by

$$y=E_{F_s}(\text{clean})-E_{\text{VBM}}(\text{clean}) -[E_{k,\text{As } 3d_{5/2} \text{ or Ga } 3d_{5/2}}(\theta) -E_{k,\text{As } 3d_{5/2} \text{ or Ga } 3d_{5/2}}(\text{clean})] .$$

For the p-type sample ($h\nu=40.8$ eV) the resolution was not sufficient to resolve the $3d_{5/2}$ component, so the shifts shown in Fig. 8 for p-type were determined from the Ga $3d$ core-level peak centroids.

For n-type sample in the "band-bending region" (less than 1 ML of Au), the Ga and As peaks move very much together and show only very small changes in shape due to chemical interaction (see Sec. III B 1). Thus we can conclude that the shift of the peak positions is due almost completely to band bending, indicating a Schottky-barrier height of $\sim$0.9 eV at 1 ML of Au coverage. At higher coverages, there is a significant amount of shifting due to chemical interactions, as evidenced by the difference in As and Ga peak positions. At these high coverages the Ga $3d$ core level exhibits the narrowing and development of a low-kinetic-energy tail described earlier in Sec. III A 1 *b*. The binding energy relative to the metallic Fermi level of the Ga $3d_{5/2}$ at 80 ML Au coverage is 18.66±0.1 eV, and the binding energy of the Ga $3d$ centroid is 18.83±0.1 eV, assuming full screening of the band-bending charge. The corresponding values for no screening are 19.51 and 19.68 eV, respectively. The binding energies of the As $3d_{5/2}$ and $3d_{3/2}$ components, assuming full screening, are 40.8 and 41.3 eV, respectively.

For p-type surfaces the peak centroid is at $\sim$19.0 eV below E_F, implying a $3d_{5/2}$ binding energy of $\sim$18.8 eV,

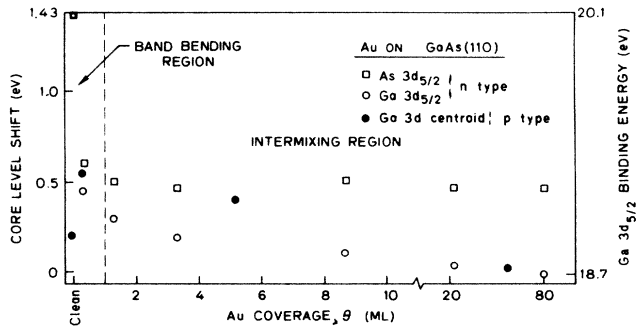

FIG. 8. As $3d_{5/2}$ and Ga $3d_{5/2}$ core-level shifts as a function of Au coverage on n-type GaAs(110). The quantity plotted on the vertical axis is equal to $E_{F_s}(\text{clean})-E_{\text{VBM}}(\text{clean}) -[E_{k,3d_{5/2}}(\theta)-E_{k,3d_{5/2}}(\text{clean})]$. For p-type $E_{k,3d\,\text{centroid}}$ of the Ga $3d$ peak is used instead of $E_{k,3d_{5/2}}$.

assuming full screening of the band-bending charge. Since the effect of band bending on the core-level binding energies for p-type surfaces is opposite to that for n-type ones, the values for no screening would be reduced to ~ 18.1 and ~ 17.9 eV, respectively. Thus the values of E_B for metalliclike Ga at high coverage as measured on n- and p-type surfaces are consistent only if nearly complete screening of the interface charge is assumed.

B. Discussion

1. Intermixing

In order to identify various chemical and physical configurations on the basis of the measured core-level binding energies presented in the preceding section, it is necessary to have accurate data of the same binding energies for well-characterized samples of the various alloys and compounds expected to be present. It is clearly impossible to have reference measurements for all possible chemical configurations of Au, Ga, and As in all possible solid (and liquid) bulk and surface phases which may occur in the system under study; we have attempted to investigate in detail only the Au-Ga surface chemistry by following the Au and Ga core-level E_B's as a function of two variables—relative Au-Ga concentration and cluster size. A compilation of the relevant data from the literature is presented in Fig. 9. The three surfaces depict the Au $5d$ splitting and the Au $4f_{7/2}$ and Ga $3d_{5/2}$ binding energies as a function of Au (Ga) atomic concentration and cluster size. It is evident that even over this limited two-dimensional space the available data are restricted to the vertical axis planes, i.e., to bulk alloys and pure Au clusters. Such data are, however, useful in suggesting trends

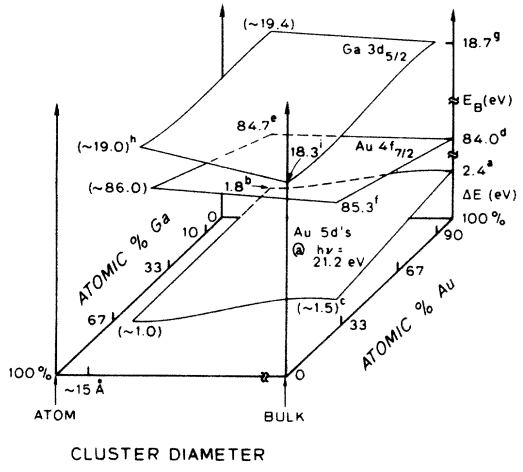

FIG. 9. Schematic diagram of experimentally determined values for the Au $5d$ splitting at $h\nu=21.2$ eV and the Au $4f_{7/2}$ and Ga $3d_{5/2}$ binding energies relative to the Fermi level as a function of cluster size and relative Au-Ga concentration. Values in parentheses represent estimates for which no known data are available. Footnoted values are as follows: *a*, Refs. 45 and 40; *b*, Ref. 40; *c*, estimate based on XPS data of Ref. 46; *d*, Refs. 47 and 48; *e*, Ref. 42; *f*, Ref. 49; *g*, Ref. 41; *h*, estimate based on Cu $3d$ data of Ref. 50; and *i*, Ref. 41.

to be expected for clusters of varying size and composition.

For submonolayer coverages Chye *et al.*[14] concluded that the Au on the surface was well dispersed and atomic-like. This conclusion was based on the splitting and shape of the Au $5d$ bands being more similar to those of atomic Au than bulk Au metal. While this rules out the presence of pure Au clusters, it does not rule out the possibility of Au-Ga alloy clusters, since alloying would also cause a decrease in the Au $5d$ splitting relative to pure bulk Au (see Fig. 9). One possibility for distinguishing between these two cases would be to observe the presence of a metallic-like component in the Ga $3d$ core-level spectrum. Our studies of the Ga $3d$ core-level spectrum using 40.8 eV (see Sec. III A 1 *b*) and those of Skeath *et al.*[51] using 30 eV show no evidence of such a state at submonolayer coverage. However, using the higher photon energy of 100 eV with the correspondingly lower background, we are able to observe subtle changes in line shape at the lower coverages. A small tail on the low-kinetic-energy side of the Ga $3d$ peak is noticeable at 0.33-ML coverage, but is too weak to resolve into a distinct peak. In order to investigate this submonolayer-coverage region further, a second cleave was made on the same sample. No change in line shape was detectable for 0.07 ML, but the tail was clearly seen at 0.7 ML. A similar tail is also seen on the As $3d$ peak. This suggests that the tail may be due to nonuniform pinning over the surface (see Sec. IV B 2 *a* for a detailed discussion of this effect), which necessarily implies that there be large distances between clusters. Consequently, we interpret this as evidence for a nonuniform distribution of Au over the surface at submonolayer coverages.

Chye *et al.*[14] also concluded that at the higher coverages the Au forms compounds or alloys with the semiconductor components. This result was based on the observation that the valence-band EDC's at $h\nu=21$ eV do not resemble bulk Au. Our data for the valence band and core levels support this general picture and, in addition, allow us to more specifically identify the products of the Au-GaAs intermixed phase. At low coverages, narrowing of the As $3d$ peak may be due to the removal of the surface-shifted peak over a portion of the surface.[52] At intermediate coverages (1 ML $<\theta<$ 15 ML) the behavior of the As $3d$ FWHM in Fig. 5 is suggestive of the presence of two As states—one from the substrate and another from dissociated As (which may be intermixed or compounded with Au). The data indicate that these states would be close in energy position (~ 0.1 eV) and would both be present for the intermediate-coverage range. Above ~ 20 ML the peak width begins to narrow, suggesting that the substrate component is being covered by the Au overlayer. This indicates that the overlayer is fairly uniform (i.e., no appreciable uncovered portions of the GaAs substrate). The $3d_{3/2}$ and $3d_{5/2}$ binding energies of 41.3 and 40.8 eV can be compared to the work of Bahl *et al.*[53] who measured the binding energies of the As core levels for an elemental metallic As sample. They obtained values of 42.1 ± 0.1 and 41.5 ± 0.1 eV for the As $3d_{3/2}$ and As $3d_{5/2}$ binding energies respectively (Roberts *et al.*[54] obtained an average As $3d$ E_B of 41.2 eV). Our measured

values (see Sec. IV A 2 *a* for more detailed measurements) are 0.8 and 0.7 eV lower. This suggests that we do not have pure bulk As metal (nor small clusters of As metal which would have even higher binding energies), assuming that metallic As would effectively screen the major portion of the interface charge. One possibility may be an As-Au interaction. For intermetallics this would result in a higher binding energy than the bulk; however, this trend may not be applicable to As, since elemental As has relatively tight, almost covalent bonds. Arsenic is known to exist in the crystalline gray (α) metallic state[53] as well as the crystalline yellow (γ) and amorphous (β) states,[55] and has been considered to be a semiconductor by some workers.[56] This behavior is similar to that of phosphorous, which also exists in a number of allotropic forms, including white, yellow, red, black (crystalline semiconductor[57]), and amorphous.[58] Thus adding Au to elemental As will tend to decrease the As core-level E_B, as observed in our data. The results of calculations of the heats of reaction of Au on GaAs for various Au-As compounds are presented at the end of this section. A somewhat similar trend in core-level E_B is seen for Pd on InP in which the metallic In 4*d* core level moves toward lower binding energy as the Pd coverage is increased.[59] This behavior, though more difficult to understand than the As case, may well be due to a similar mechanism. One final possibility is that the peak is due to an elemental form of As (perhaps semiconducting) with essentially no screening of the interface charge. In this case we may have to add the band-bending value of 0.85 eV to our measured E_B, resulting in a value close to that of Bahl *et al.*[53] However, due to the large amount of metallic Au and Ga present at these coverages it seems unlikely that the interface charge would be so incompletely screened (see following discussion).

In the higher-coverage region ($\theta > 15$ ML) the Ga 3*d*, Au 4*f*, and Au 5*d* spectra indicate the formation of a Au-rich Au-Ga alloy of bulk or large-island morphology. Our measured splitting of the Au 5*d*'s at 21.2 eV is $\sim$2.35 eV. A splitting of $\sim$2.4 eV is observed for pure Au at 21 eV.[45] Our value for the splitting between the two prominent peak maxima is $\sim$1.9 eV as compared to $\sim$1.7 eV for pure Au.[45] Thus our valence-band data support the conclusion of Chye *et al.*[60] that the Au overlayer structure is similar but not identical to that of pure bulk Au. This splitting can be due to a bulklike Au-Ga alloy or to clusters of more than several hundred atoms of pure Au.[40] For pure Au this splitting remains fairly constant as large (bulklike) clusters decrease in size, and itself begins to decrease only for clusters of fewer than $\sim$200 atoms (diameter $\sim$24 Å); however, the height of the low-binding-energy (-4.3 eV) peak is greater than that of the higher- (-6.2 eV) binding-energy peak for all cluster sizes, including bulk Au.[40] Since our data for 25×10^{15} atoms/cm^2 show the opposite trend, we may conclude that we are not observing pure Au in either bulk or cluster form. Nicholson *et al.*[41] have measured the Au 5*d* binding energies at $h\nu=40.8$ eV for bulk Au-Ga alloys of various compositions and have found that the Au 5*d* splitting decreases from 3.2 to 1.3 eV in going from pure bulk Au to a bulk $Au_{33}Ga_{67}$ alloy. Hufner *et al.*[46] see a decrease from 2.8 to 1.6 eV at $h\nu=1253.6$ eV. A similar decrease in splitting is seen in the XPS data of van Attekum *et al.*[46] for a Au-Ga_2 compound. On the basis of our measured 5*d* splitting we can thus conclude that we are observing a Au-rich Au-Ga alloy.

The two possible morphologies of Au-Ga intermixing just described—bulk or large clusters—are also consistent with the measured Au 4*f* and Ga 3*d* core-level binding-energy values. The Ga $3d_{5/2}$, $3d_{3/2}$, and weighted average binding energies are measured to be 18.27, 18.75, and $\sim$18.5 eV for Ga_{100} and 18.71, 19.04, and $\sim$18.8 eV for $Au_{90}Ga_{10}$, respectively.[41] Our measured values are 18.66 and 18.83 eV for the $3d_{5/2}$ and peak centroid binding energies using the total peak and assuming full screening of the band-bending charge. Thus our data are consistent with the formation of a bulklike $Au_{90}Ga_{10}$ alloy (approximate composition) in which the metallic charge completely screens the semiconductor interface charge. The possibility of partial screening, however, must also be considered. In this case our measured value of the Ga 3*d* binding energy would be increased, and therefore may correspond to a slightly more Au-rich alloy (see Fig. 9). Another mechanism for giving an increased E_B is a decreased cluster size. It is well known from studies on many different metals (see Refs. 61 and 62 and references therein) that the *d*-electron binding energy increases as the particle size decreases. These shifts are of the order of 1 eV. Thus both the Au 5*d* and Ga 3*d* spectra are also consistent with the formation of medium-to-large-scale clusters.

Our value for the Au $4f_{7/2}$ binding energy at 80 ML is 84.0 eV. This is equal to the value observed by others for pure Au,[47,48] although some have used a value of 83.8 eV.[42,63] We also observe a distinct narrowing of the linewidths of the two 4*f* components as the coverage is increased; this effect has been observed for the growth of metal clusters toward the bulk.[61] It is also known that the Au 4*f* binding energy increases with decreasing cluster size (by 0.7 eV from bulk to 15-Å-diameter clusters) (Ref. 42) and decreasing Au concentration in the Au-Ga alloy.[49] Thus our Au 4*f* data are also consistent with the two possible growth modes discussed above.

We thus conclude, on the basis of the Au 5*d*, Ga 3*d*, and Au 4*f* core-level spectra, that the growth and intermixing of the Au overlayer result in the formation of a Au-rich Au-Ga alloy in the form of medium-to-large-scale bulklike clusters. The growth of tightly packed overlapping clusters of Au on an Al(100) substrate has been observed by Egelhoff.[64,65] The presence of large uncovered portions of the GaAs substrate is unlikely, as indicated by the narrowing of the As 3*d* and Ga 3*d* peaks; however, the core-level emission from small uncovered regions of the substrate ("pinholes") may be masked by thick islands due to the large off-normal (42.6°) collection angle of the CMA. The high-binding-energy tail on the As 3*d* peak has been suggested as being due to a bulk As contribution.[14] Another possibility, which has been suggested to explain a similar behavior of the P 2*p* core level for various metals on InP(110) (Ref. 66) is that the gradual growth of the high-kinetic-energy tail may be due to the presence of a metal-anion compound of continuously

varying composition. Such an effect is particularly applicable to systems in which a low heat of formation of the metal compound leads to a kinetically limited nonequilibrium reacted phase.

It is of interest to compare our observations to the predictions of bulk thermodynamics for the Au-GaAs system. Such a model has been used to successfully predict the reactivity (heat of reaction) of a number of metals on GaSe and InP using known values of the heats of formation of metal-anion compounds and the alloying enthalpies of metal-cation alloys.[67] We have made use of calculated values of the heats of formation of various Au-As compounds,[68,69] to calculate the heat of reaction (see Appendix A). We find that the interface is reactive for all tabulated Au-As compounds ($AuAs_5$ through Au_5As) when metal alloying at infinite dilution is included. The interface is not reactive for any of the tabulated Au-As compounds if alloying is not included. The lowest heats of reaction correspond to formation of $AuAs_5$ or $AuAs_2$. We find also that the Cu-GaAs interface is reactive for Cu_2As or Cu_3As formation in both the infinite dilution and equiatomic limits, while the Ag-GaAs interface is not reactive for any of the tabulated compounds in either limit.

2. Fermi-level pinning

As discussed in the preceding section, it is clear that for coverages greater than ~ 1 ML both the As $3d$ and Ga $3d$ core-level spectra contain contributions from more than simply the undisturbed substrate. As a result the band bending, as measured by the shifts of these core levels, can only be followed with confidence for coverages <1 ML. This is indicated in Fig. 8 by the dashed line dividing the data into the "band-bending" region and the "intermixing" region. For the band-bending region our measured value of the Schottky-barrier height is 0.85 ± 0.1 eV. At 0.33 ML Au coverage the shift of the As $3d$ gives a value of 0.82 eV and that of the Ga $3d$ gives a value of 0.95. Thus it is clear that even at this low coverage the effects of intermixing are beginning to be seen. This value of the barrier height can be compared with I-V and C-V measurements of similarly prepared (UHV) thick diodes.[30] The values reported there were 0.92 eV for I-V and 0.99 eV for C-V measurements. Slightly lower (by ~ 0.05 eV) values were measured for Ag and Cu.

Based on the results of photoemission studies for a large number of metal-GaAs interfaces, a model has been proposed which attributes the observed pinning on n- and p-type surfaces to defect-related states which are induced by the deposition of an adatom (which may be either a metal or oxygen).[14,12,70,71] This model, known as the unified defect model (UDM),[72] established an acceptor defect level at 0.75 eV above the VBM and a donor level at 0.5 eV above the VBM. For most metals studied earlier the pinning has been observed to occur at the acceptor level for n-type surfaces and the donor level for p-type surfaces.[71] Only Au, and more recently, Cu, Ag, and Pd show pinning for n-type samples at this lower level.[73,30,74] This suggests that the mechanism for barrier height determination must involve a property of the metal atoms in addition to the presence of the defect levels. It has been suggested that for metals with large electron affinity a removal of electrons from the defect levels by the metal may allow for pinning of n-type GaAs at the donor level.[75,30]

IV. HEATING OF THE Au-GaAs INTERFACE

In the preceding section we have shown that deposition of Au onto the clean GaAs(110) surface under UHV conditions results in a barrier height of ~ 0.9 eV. It is well known, however, that the thermal processing which forms a necessary step in many device fabrication procedures leads to lowered barrier heights on chemically prepared, oxide-covered wafer surfaces (see Sec. I). In this section we present and discuss photoemission data on Au-GaAs interfaces prepared and thermally processed in UHV. We also discuss I-V and C-V data on similarly prepared and heat-treated structures. In this way we can isolate the essential physical processes occurring at the interface which lead to lowering of the Schottky-barrier height.

A. Results

1. Low coverage (0.2 ML)

We studied the effects of heating on 0.2-ML-thick Au overlayers on both n- and p-type GaAs(110) surfaces using 21.2 and 40.8 eV light from a monochromatized He-discharge lamp source (see Sec. II). This source is ideally suited to studies in the low-coverage regime where the substrate signal is strong and where the high cross section for photoemission from the VB region at $h\nu=21.2$ eV allows for accurate and direct measurements of the movement of E_{F_s}. This movement is also observed in the shift of the substrate Ga $3d$ core level which remains largely unaffected by the low Au coverage. The photoemission investigation presented in this section must be distinguished from other reported heat-treatment experiments because we have studied a very thin (0.2 ML) Au film on the clean surface. Therefore, the effects of interdiffusion of Ga into Au will be different from those observed with very thick Au films (>2000 Å) on oxide-covered GaAs surfaces.[8] The movement of E_{F_s} will also be somewhat different from that for thicker Au films (see Sec. IV A 2) due to the fact that E_{F_s} for 0.2 ML of Au has not yet stabilized at its final value.

The valence-band spectra for 0.2 ML of Au on GaAs(110) are shown in Fig. 10 for n-type samples and in Fig. 11 for p-type ones. The initial annealing of the clean surface appears to remove the defects due to cleaving. This causes E_{F_s} to become less pinned on both n- and p-type surfaces. This effect can be seen on the valence-band EDC's where the structure at 5.0 eV below E_{F_s} for the heated surface becomes sharper than that for the cleaved clean surface. Deposition of 0.2 ML of Au on the surface results in an additional peak at an energy of ~ 4.5 eV below E_{F_s} due to emission from the Au $5d$ core levels.

The first heat treatment of the Au overlayer at 100 °C results in no noticeable change in the VB structure. After

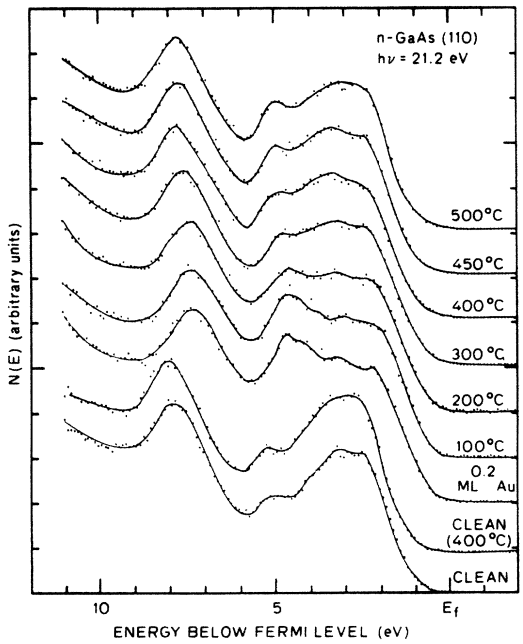

FIG. 10. Photoemission energy distribution curves of the valence-band region for n-type GaAs(110) taken at room temperature with a photon energy of 21.2 eV after heating to the indicated temperatures. The 0.2-ML Au overlayer was deposited on the clean surface at room temperature.

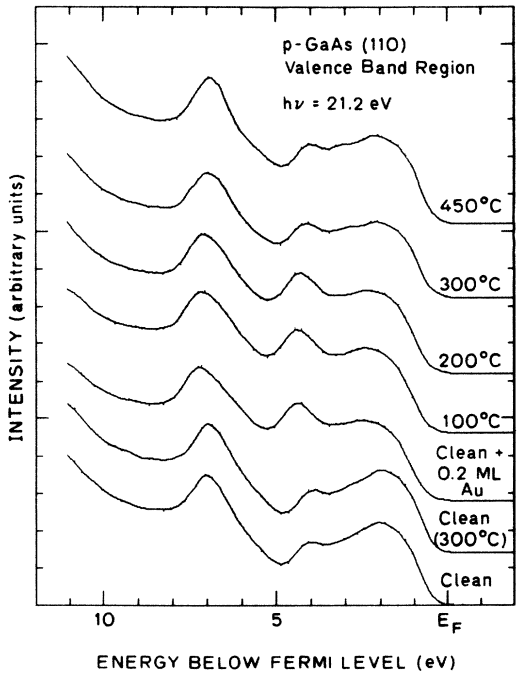

FIG. 11. Photoemission energy distribution curves of the valence-band region for p-type GaAs(110) taken at room temperature with a photon energy of 21.2 eV after heating to the indicated temperatures. The 0.2-ML Au overlayer was deposited on the clean surface at room temperature.

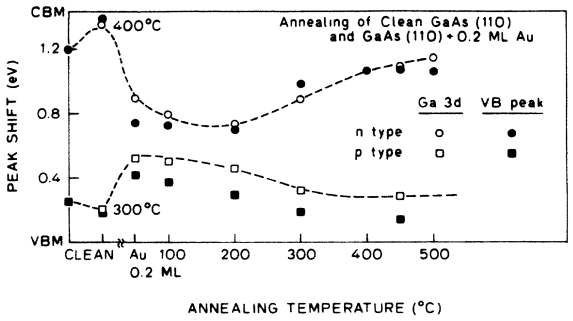

FIG. 12. Fermi-level pinning position for 0.2 ML Au on n- and p-type GaAs(110) based on the valence-band ($h\nu=21.2$ eV) and Ga $3d$ core-level ($h\nu=40.8$ eV) peak maximum positions.

the 200 °C anneal, however, there is a decrease in the Au-related peak and a slight shift of the entire VB structure toward higher binding energy. This shift, as followed by the prominent valence-band peak at 6.75 eV below the VBM, continues as the sample is heated to higher temperatures.

The shift of the 6.75-eV valence-band peak, as well as the shift of the Ga $3d$ core-level peak maximum, is plotted in Fig. 12 for both n- and p-type surfaces. On n-type GaAs the initial heating at 400 °C of the clean surface caused E_{F_s} to move closer to the conduction-band minimum (CBM) by about 0.2 eV. Deposition of 0.2 ML of Au caused E_{F_s} to drop by ~ 0.5 eV. Heating to 100 °C and 200 °C left E_{F_s} essentially unchanged. After heating to 300 °C, E_{F_s} moved upwards by ~ 0.15 eV. After heating to 500 °C, E_{F_s} returned close to its position on the clean surface. On p-type surfaces the movement of E_{F_s} is similar. An initial heating to 300 °C of the clean surface caused E_{F_s} to drop. Deposition of 0.2 ML of Au caused E_{F_s} to move up by 0.5 eV. Heating of the Au-GaAs interface resulted in E_{F_s} movement towards its position on the clean surface.

2. *High coverage (15 ML)*

In this section we present photoemission results on the heating of a relatively thick (15 ML) Au overlayer on GaAs(110). These results can be more readily compared to those on thick (~ 1000 Å) devices since E_{F_s} is stabilized. Since intermixing becomes important at these coverages, it is necessary to use a photon energy high enough to monitor both the Ga $3d$ and As $3d$ as well as the Au $4f$ core levels in order to follow the effects of the interaction. We have thus used synchrotron radiation to provide the required photon energies. During this experiment only the n-type surface was studied (see Sec. II).

a. Energy distribution curves. Photoemission spectra for the Ga $3d$ core level are shown in Fig. 13. The spectrum labeled "clean" was taken immediately after cleaving. The sample was then heated to 500 °C for 15 min and then allowed to cool to room temperature before the next spectrum was taken. This shows a slight movement of E_{F_s} by about 0.1 eV towards the conduction-band

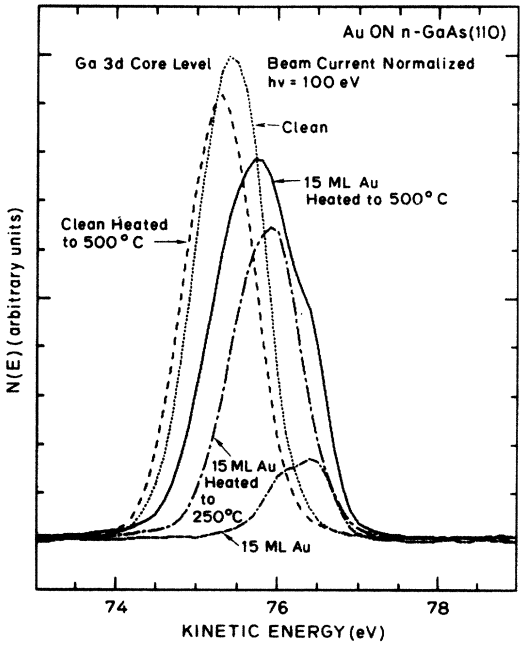

FIG. 13. Photoemission spectra of the Ga $3d$ core level taken at room temperature with a photon energy of 100 eV after heating to various temperatures. The Au was deposited on the clean surface at room temperature.

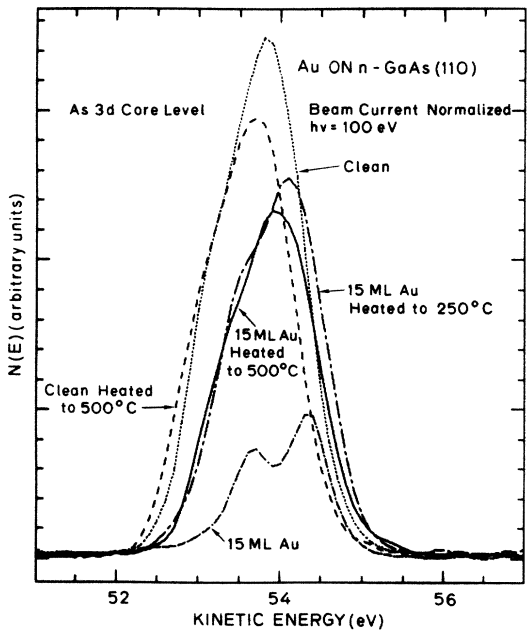

FIG. 14. Photoemission spectra of the As $3d$ core level taken at room temperature with a photon energy of 100 eV after heating to various temperatures. The Au was deposited on the clean surface at room temperature.

minimum, with no observable change in shape. This is similar to the effect seen in the preceding section for clean GaAs. The 15-ML Au layer was then deposited (at room temperature) and a spectrum taken. Again we see the large band-bending shift as well as the effects of Au intermixing. The binding energy of the centroid of this Ga peak is determined to be 18.90 ± 0.1 eV and the binding energy of the Ga $3d_{5/2}$ is 18.64 eV, assuming full screening as described for the room-temperature data in Sec. III A 2 *b*. After heating to 250 °C the peak moves to higher binding energy and returns to the peak shape of the clean surface with no noticeable difference. After heating to the highest temperature of 500 °C, the peak has developed a low-binding-energy shoulder suggestive of metallic Ga. This structure is analyzed in further detail in the next section.

The As $3d$ core level is shown in Fig. 14. The general behavior is similar to that of the Ga, except for two important differences. After the Au deposition the As $3d$ peak becomes narrower and two distinct components are seen. [These peaks are better resolved than those for a similar coverage in the room-temperature experiment because of the higher CMA resolution used during the heating experiment (0.175 eV versus 0.35 eV).] We find a splitting of 0.66 eV between the two spin-orbit components and a peak height ratio of 1.32. The measured binding energies relative to E_F assuming full screening are 40.72 eV for the $3d_{5/2}$ and 41.38 eV for the $3d_{3/2}$. We also find that the peak shape after heating of the Au-covered surface to 500 °C is indistinguishable from that of the as-cleaved clean surface, while the 250 °C heat treatment produced is a small tail at lower E_k that is not observed in the spectrum of the clean surface. The Au $4f$ core levels for the as-deposited room-temperature surface and the surface after heating to 500 °C are shown in Fig. 15. The $4f_{7/2}$ binding energy for the as-deposited surface is 83.95 ± 0.1 eV and for the annealed surface is 84.45 ± 0.1 eV.

Photoemission spectra of the VB region taken with a photon energy of 120 eV are shown in Fig. 16. The shift of the VBM to higher binding energy after heating of the clean surface to 500 °C is clearly seen in curves 1 and 2. Heating of the Au-covered surface results in a decrease in the Au $5d$ splitting and a shift of both levels to higher binding energy. After heating to 500 °C we note the appearance of a Fermi edge as well as a small shoulder that corresponds closely to the clean GaAs valence-band structure.

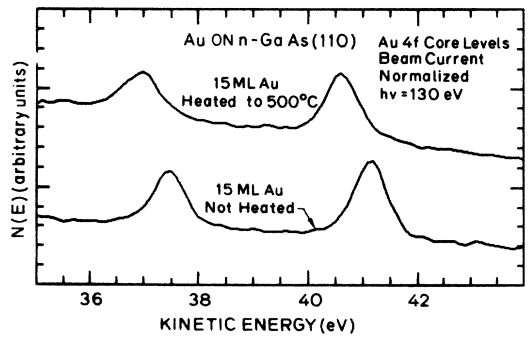

FIG. 15. Photoemission spectra of the Au $4f$ core levels taken at room temperature with a photon energy of 130 eV immediately after deposition (no heating of the Au, lower curve) and after heating to 500 °C (upper curve).

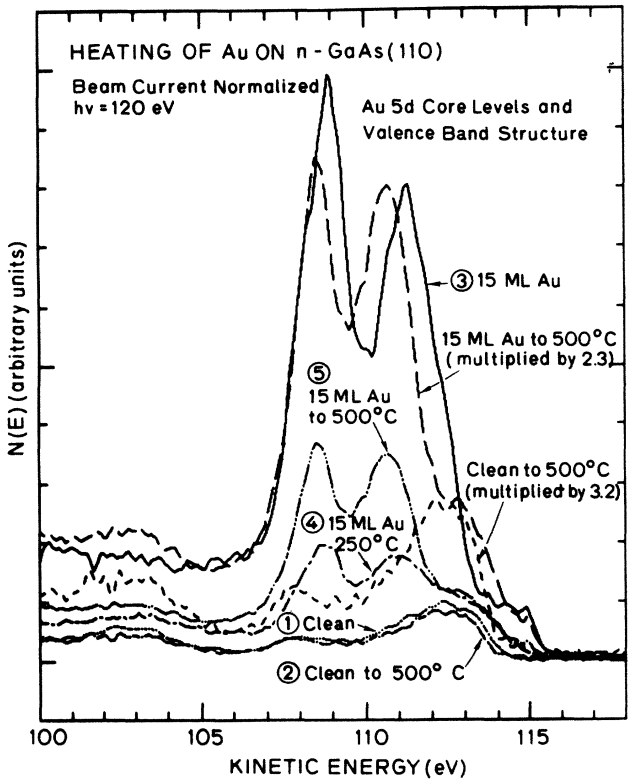

FIG. 16. Photoemission spectra of the valence-band region taken at room temperature with a photon energy of 120 eV after heating to various temperatures. Each step in the surface treatment is numbered in chronological order. The Au was deposited on the clean surface at room temperature. Enlarged curves are included for the clean surface heated to 500°C (multiplied by 3.2) and for the Au-covered surface heated to 500°C (multiplied by 2.3).

b. Results derived from EDC's. The Ga $3d$/As $3d$ core-level intensity ratio is shown in Fig. 17. The initial ratio is 0.92 and increases slightly to 1.0 after heating (this ratio was 1.05 for the clean cleave in the room-temperature experiments). After the 15-ML Au deposition the ratio drop dramatically to 0.6 (similar to the value of 0.56 in the room-temperature experiment at 23 ML as determined from the data of Fig. 6). After heating to 250°C this ratio increases to 0.82 and after 500°C to 1.38.

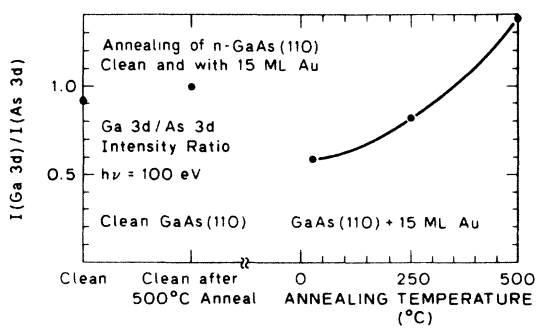

FIG. 17. Ga $3d$/As $3d$ total peak core-level intensity ratio plotted for each step in the sample processing.

The Ga $3d$ peak shows a significant shoulder on the lower-binding-energy side after heating of the Au-covered surface to 500°C. In order to investigate this peak further we performed a curve fitting procedure on the peak using two components with shape equal to that of the clean surface [see Fig. 18(a)]. Using the clean peak shape to model the shifted component is not completely satisfactory since the clean peak contains a surface-shifted component which would not be present for a disordered metallic phase; therefore, we have also performed a curve fitting using the Ga $3d$ peak for the 15-ML deposition at room temperature to more accurately represent the disordered metallic phase [Fig. 18(b)]. For the first curve fitting [Fig. 18(a)] we find that the two peaks are shifted by 0.67 eV and the binding energy of the centroid of peak "B" is 18.89 eV relative to E_F, assuming full screening from the interface charge. This corresponds to a binding energy for the Ga $3d_{5/2}$ component of $\sim$18.7 eV. The ratio of the area of peak B to that of the Ga $3d$ peak for 15 ML of Au at room temperature is 2.7. The ratio of the substrate component (peak A) area to that of the As $3d$ peak for the same surface (15 ML Au heated to 500°C) is 0.80. For the second curve fitting [Fig. 18(b)], we find a centroid splitting between the two components of 0.55 eV.

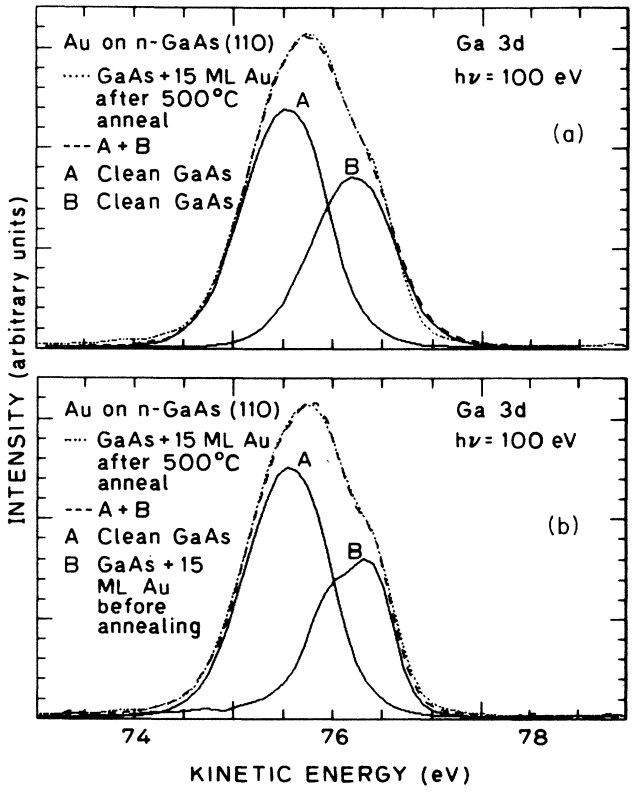

FIG. 18. Curve fitting of the Ga $3d$ peak for the GaAs(110) surface with 15 ML Au heated to 500°C using the Ga $3d$ peak from (a) the clean surface and (b) the surface with 15 ML Au at room temperature to represent the shifted Ga component.

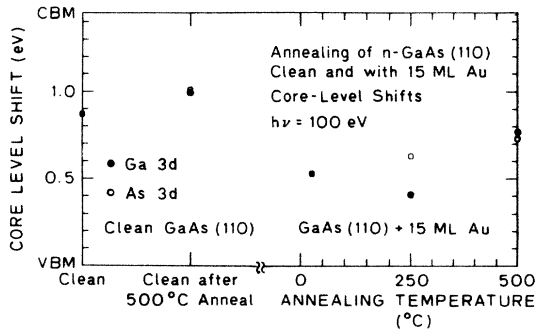

FIG. 19. Fermi-level position for heating of 15 ML of Au on n-type GaAs(110) as determined from the As $3d$ and Ga $3d$ core-level shifts. The value for the 15-ML Au deposition at room temperature is taken from the data of Fig. 8.

The binding energy of the Ga $3d_{5/2}$ component of peak B is 18.76 eV. The ratio of the area of peak B to that of the total Ga $3d$ peak for 15 ML of Au at room temperature is 2.4. The ratio of the area of peak A to that of the As $3d$ peak for the same surface is 0.83.

Because of the strong indication that the substrate surface becomes largely uncovered after heating of the Au overlayers, particularly at 500 °C, it becomes possible to consider following the band bending at the surface by observing shifts the now-exposed substrate core-level peaks (the VBM remains obscured by emission from the Au Fermi edge even after heat treatment, as seen in Fig. 16). It should be noted that the presence of chemically shifted peaks lying close to the energy position of the substrate can give rise to a total peak with a shape very similar to that of the substrate and that this makes it very difficult to deconvolve the substrate peak to determine the band bending. The movement of E_{F_s} is shown in Fig. 19. We find that E_{F_s} on the clean surface was initially pinned at 0.87 eV above the VBM and increased slightly to 1.0 eV after heating. After the initial 15-ML Au deposition it becomes impossible to determine the band bending from the photoemission spectra since the substrate core levels are completely covered. We have thus assumed the accepted barrier height of $\sim$0.9 eV to locate E_{F_s} for this coverage. After heating to 250 °C we see an upward shift of 0.08 eV, as measured by the As $3d$ peak, and a downward shift by $\sim$0.14, as measured by the Ga $3d$ one. After heating to 500 °C the As peak shape becomes indistinguishable from that of the clean peak and indicates an E_{F_s} position of 0.73 eV above the VBM. For the Ga $3d$ peak at this temperature we obtain a value for E_{F_s} of 0.77 eV above the VBM from the curve fitting of Fig. 18(a) and 0.73 eV above the VBM from that of Fig. 18(b). This latter value gives a barrier height of 070 eV.

B. Discussion

1. *Intermixing*

The effect of heating on the submonolayer (0.2 ML) Au-covered surface can be explained as either a clustering of the Au into relatively thick islands (>10 Å) or deep diffusion of Au into the substrate. Both of these behaviors would lead to the reduction in observed Au $5d$ intensity, as seen in the spectra of Fig. 10. The clustering effect may be the more plausible one given the strong clustering seen for the higher coverage (15 ML) heating experiment (see below).

The development of the Au overlayer with increasing temperature for the 15-ML coverage shows a strong indication of Au clustering and increasing Ga concentration. That is to say that a Au-rich (e.g., $Au_{90}Ga_{10}$) largely uniformly distributed bulklike layer is initially formed after deposition of 15 ML of Au at room temperature, as seen in the room-temperature experimental results presented and discussed in Sec. III. This relatively low Ga concentration is roughly consistent with the known low solid solubility of Ga in Au at room temperature.[76] The presence of a segregated As component on or near the surface is evidenced by the large (1.7) As-to-Ga ratio for this coverage at room temperature (see Fig. 17). After heating to 250 °C there still remains some segregated As, as indicated by the As-to-Ga ratio of 1.2, yet both the As the Ga peak shapes show strong substrate contributions. This indicates that large portions of the clean surface have become exposed due to agglomeration of the Au. After heating to 500 °C this As has been removed (probably by evaporation), the Au has formed clusters, and the metallic Ga concentration has increased.

Loss of As is shown by the large decrease in As/Ga ratio (from 1.2 to 0.7). Au clustering is indicated by the shift of the Au $4f$ levels to $\sim$0.4 eV higher binding energy after heating. It is well known that relatively thin ($\sim$4 ML) extended surface layers can give bulklike binding energies, whereas clusters must reach larger ($\sim$20 ML) diameters before exhibiting bulk properties.[64] Oberli *et al.*[42] have shown that Au clusters of $\sim$100 Å diameter exhibit $4f_{7/2}$ binding energies greater by 0.12 eV than those of the bulk, and clusters of 25 to 60 Å diameter give a corresponding shift of 0.2 eV. Since addition of Ga to pure Au clusters also leads to an increase in the Au $4f$ binding energy (see Sec. III B 1 and Fig. 9), our data are consistent with the formation of Au-Ga alloy or compound clusters after heating to 500 °C. This conclusion is further supported by the behavior of the Au $5d$ levels. Both the decrease in splitting (see Fig. 9 and Ref. 41) and the shift of both levels to higher binding energy[41] are seen when the Ga concentration is increased.

Additional evidence for this model of the Au-Ga morphology can be obtained from the binding energy of the deconvolved metallic Ga component after 500 °C heating. Using the approach described in Sec. III, we obtained a Ga $3d_{5/2}$ E_B of 18.7 eV. This corresponds closely to the Ga $3d_{5/2}$ binding energy observed immediately after the 15-ML Au deposition at room temperature. The intensity of the metallic Ga peak after heating is, however, $\sim$2.7 times the intensity of the RT value. Clusters with such an increased Ga concentration would be expected to give a binding energy in the range of $\sim$18.5–19.2 eV; thus, our observed value is consistent with the formation of Au-Ga alloy or compound clusters after heating, as described above.

2. *Fermi-level pinning*

a. Low coverage (0.2 ML). The data described in Sec. IV A 1 can be summarized as follows for an *n*-type GaAs(110) surface.

The clean cleaved surface was initially pinned at a barrier height of 0.2 eV.

Heating of the clean surface to 400 °C reduces the measured barrier height to ~0.1 eV.

The deposition of 0.2 ML Au at room temperature results in a measured barrier height of ~0.7 eV that remains relatively stable after annealing to 100 and 200 °C.

Annealing to temperatures above 300 °C results in a reduction of the measured barrier height to ~0.3 eV.

In the following discussion, the amount of pinning refers to the extent to which the Fermi level has moved in energy away from its value for the unpinned surface. The initial decrease of pinning after heating of the clean cleaved surface has been observed for both *n*- and *p*-type samples and in both the low- and high-coverage experiments, and appears to be due to annealing of the defects present on the as-cleaved surface. Monch *et al.*[77] have suggested that a deep acceptor due to Cr^{2+} impurities diffuses out to the surface after heating to 800 K. Such a level would not account for the observed change in pinning position (which would require outdiffusion of a shallow donor for *n*-type surfaces and a shallow acceptor for *p*-type surfaces).

The pinning at a barrier height of 0.7 eV after 0.2 ML of Au deposition is close to that of the acceptor level observed to cause pinning for a wide range of metals on GaAs(110).[72] However, given the existence of a pinning level at ~0.9 eV below the CBM (as discussed in Sec. III B 2), this suggests the possibility that if the number of such levels is small enough, then pinning may occur at a value intermediate between zero and 0.9 eV. After heating to temperatures above 300 °C the barrier height is reduced to 0.3 eV. One possible explanation, combining this idea with that of the previous paragraph, is that a portion of the levels (at 0.9 eV below the CBM) which initially accounts for the pinning at 0.7 eV is annealed out after heating to result in the lower intermediate barrier height of 0.3 eV. Another possible effect is that of nonuniform pinning over the surface, particularly in cases where the distribution of Au over the surface is highly nonuniform and the distance between Au clusters is large compared to the diameter of the depletion boundary associated with a defect level,[78] e.g., for low coverages at room temperature and for both low and high coverages after heating. This situation is reflected in photoemission data in the following way. The VBM edge observed in the valence-band spectrum and used to locate the VBM (by linear extrapolation of the straight, high-kinetic-energy edge) corresponds to those regions of the surface for which the VBM is closest to the Fermi level; the VBM for other regions (where the pinning position is different) will occur at lower kinetic energies and so will be masked by the valence-band structure. Thus, for *n*-type samples our measured VBM position corresponds to the regions that are *most pinned;* regions with less pinning (E_{F_s} closer to the CBM, farther from the VBM) will have a VBM at lower kinetic energies. This also results in a tailing of the Ga and As 3*d* core levels to lower E_k if most of the surface is pinned at the position indicated by the observed VBM. Conversely, for *p*-type samples the observed VBM corresponds to the *least pinned* portion of the surface; regions with more pinning (E_{F_s} farther above the VBM) will have a VBM at lower E_k than the observed VBM edge.

Assuming the pinning at low coverage to be due to a level at 0.7 eV below the CBM, the above results, taken together with the observed decrease in Au 5*d* emission for temperatures $\geq$200 °C, are consistent with the assignment of this defect in the UDM to an acceptor related to missing As, which is induced by the Au atoms but does not directly involve the Au atoms in the defect complex (see Sec. IV B 2 *b* for further discussion of this defect as it relates to the higher coverage data). This type of defect would be annealed out independently of the Au cluster formation. A more detailed interpretation of the valence-band data would suggest that the Au begins to cluster at 200 °C, followed by annealing of the defects at or above 300 °C. A very similar interpretation fits well for the *p*-type data. Pinning after the initial Au deposition is at the UDM donor level at 0.5 eV above the VBM and remains there after heating to 100 °C and 200 °C. Above 300 °C the Fermi level moves back to ~0.3 eV above the VBM. Thus the decrease in barrier height occurs within the same temperature range as for *n*-type sample and therefore suggests that the donor and acceptor levels are annealed out at similar temperatures.

b. High coverage (15 ML). The effect of heating on the Schottky-barrier height for 15 ML of Au is less easy to follow because of the presence of the thick Au layer initially and reacted As and Ga phases after heating. This is indicated by the different values for the As and Ga shift at 250 °C. After heating at 500 °C, however, we can be reasonably confident that we are observing the Fermi-level position as measured by the substrate core-level peak positions. This is due to the fact that, as discussed in Sec. IV B 1, after heating to 500 °C, the reacted As has been removed (presumably by evaporation) and only the substrate peak is seen. We find that the curve-fitting procedure described in Sec. IV A 2 *a* yields a "substrate" Ga 3*d* component peak. The difference between the binding energy of this peak and that of the As 3*d* peak is characteristic of the clean substrate, thus supporting the conclusion that the As 3*d* spectrum observed after heating to 500 °C is due entirely to the uncovered GaAs substrate. Identical trends are seen in *I-V* measurements on thick (~1000 Å) Au films on cleaved *n*-type GaAs(110) surfaces prepared in UHV and annealed in a N_2 environment.[31] These measurements show a barrier height decrease from 0.92 to ~0.8 V after heating to temperatures above 300 °C.

The initial pinning after 15 ML of Au deposition may be explained by a depletion of electrons from the donor defect by the Au atoms[75,31] (see Sec. III B 2). This is also consistent with the arguments of Zur *et al.*[43] The step in pinning from 0.7 to 0.9 eV at ~0.3 ML has also been observed by Chye *et al.*[14] and suggests that perhaps a critical cluster size is necessary before pinning at the donor level can occur. Also to be considered is the possibility of Au antisite (Au replacing Ga) formation.[79]

After heating we observe evidence of strong clustering, and the Ga and As $3d$ core-level shapes and binding energies indicate that we are seeing a clean (there may be small amounts of surface Ga and/or Au in these regions) GaAs surface in addition to metallic Ga from the Au-Ga alloy clusters. This is particularly evident from the narrowness of the As $3d$ peak. Thus, we are not sensitive to the Fermi-level pinning position directly beneath the thick clusters (particularly if the distance between clusters is greater than the diameter of the depletion boundary, as discussed in the preceding section). Therefore, we can say that the pinning position of the clean surface has returned to 0.7 eV, and so the pinning again becomes dominated by the acceptor levels discussed above (no Au left to deplete donors). The I-V measurements of Newman *et al.*[31] are, however, sensitive to the barrier height of thick Au layers on cleaved GaAs(110) and they see a similar reduction with heating, as mentioned above. They suggest that this reduction may be due to Ga or Au-Ga alloy formation at the interface, which is consistent with our observations based on photoemission data. The argument that pinning is due to the presence of Au antisite point defects is weakened, due to the fact that, if this were the dominant pinning mechanism, we would expect the pinning position to remain at 0.5 eV above the VBM, since such defects would be expected to increase in number with increasing temperature as the solubility of Au in GaAs increases.

V. SUMMARY AND CONCLUSIONS

Detailed photoemission studies have been performed on the Au-GaAs(110) interface at room temperature and after annealing at temperatures up to 500 °C. The spectra of the core levels and valence-band region reveal that a significant amount of intermixing takes place, even at room temperature. The data indicate the formation of a Au-rich Au-Ga alloy in the form of medium-to-large-scale (bulklike) clusters with possible As intermixing. The degree of intermixing increases with annealing temperature, as the clusters become thicker and more enriched in Ga. At 500 °C the As evaporates, large portions of the GaAs surface become uncovered, and evidence of a nearly pure metallic Ga phase is seen.

The Fermi-level pinning behavior has also been deduced from the photoemission data. We observe pinning at a barrier height of 0.7 ± 0.1 eV for small (~0.2 ML) coverages and 0.85 ± 0.1 eV for coverages greater than ~0.3 ML on n-type GaAs(110) at room temperature. We suggest that the pinning at 0.7 eV is due to an acceptor defect level and the pinning at 0.85 eV is due to a donor defect level which, due to depletion of electrons from the defect level by the Au clusters, acts effectively to pin E_F on n-type GaAs. These levels are in agreement with those of the unified defect model. After heating of these films we observe a reduction in the amount of pinning due to annealing of defects and exposure of large portions of the surface. Pinning on p-type surfaces is observed at 0.5 ± 0.1 eV above the VBM for a coverage of ~0.2 ML at room temperature and is attributed to the same donor level. This pinning is also seen to decrease with increased annealing temperature.

APPENDIX: BULK THERMODYNAMIC HEATS OF REACTION

It is of interest to be able to predict which metal semiconductor interfaces are likely to result in chemical reaction. McGilp[67] has used bulk thermodynamic data to determine the heat of reaction, ΔH_R, for a semiconductor A_pB_q reacting with a metal M to form a compound M_rB_s and an alloy A_xM_y. The starting point is the stoichiometric equation

$$sx\,A_pB_q+(qrx+psy)M\rightarrow qxM_rB_s+psA_xM_y\ . \qquad \text{(A1)}$$

We note that this equation assumes that the semiconductor is completely consumed (i.e., equilibrium is reached) and that only two phases are produced (three phases are possible in general[80,81]).

Normalizing to unit metal atom involved in compound formation and setting $p=q=1$, we obtain the following three limiting cases.

(i) For systems where alloying is energetically unfavorable the heat of reaction is given by (see McGilp[67])

$$\Delta H_R^{(3)}=(1/r)\Delta H_f^{\ominus}(M_rB_s)-(s/r)\Delta H_f^{\ominus}(AB)\ , \qquad \text{(A2)}$$

where $\Delta H_f^{\ominus}$ is a standard heat of formation.

(ii) For equiatomic metal alloy formation,

$$\Delta H_R^{(4)}=(1/r)\Delta H_f^{\ominus}(M_rB_s)+(s/r)\Delta H_f^{\ominus}(AM)-(s/r)\Delta H_f^{\ominus}(AB)\ . \qquad \text{(A3)}$$

(iii) For infinite dilution of A in M,

$$\Delta H_R^{(5)}=(1/r)\Delta H_f^{\ominus}(M_rB_s)+(s/r)\Delta H_{\rm sol}(A;M)-(s/r)\Delta H_f^{\ominus}(AB)\ , \qquad \text{(A4)}$$

where $\Delta H_{\rm sol}(A;M)$ is the heat of solution of A in M for the solid alloy at infinite dilution.

McGilp[67] has presented values for the above quantities for various metals on GaSe and InP, assuming formation of the "most stable" selenide (and presumably phosphide) phases. We present here values for the above quantities for Au, Ag, and Cu on GaAs for a range of possible arsenide compounds. We also use two sets of values for $\Delta H_f^{\ominus}(AM)$ and $\Delta H_{\rm sol}(A;M)$. One set consists of the values used by McGilp[67] calculated using the theory of Miedema *et al.*[82] The other set is taken directly from the tabulated results of calculations by Niessen and Miedema[68] and Niessen *et al.*[69] Values for $\Delta H_f^{\ominus}(M_rB_s)$ are taken from the calculated values of Niessen and Miedema[68] and Niessen *et al.*[69] and the experimentally determined values of Kubaschewski and Alcock[83] and Wagman *et al.*[84] Values for $\Delta H_f^{\ominus}(AB)$ are taken from Kubaschewski and Alcock.[83] All values of $\Delta H_f^{\ominus}$ and $\Delta H_{\rm sol}$ are expressed in units of eV/molecule, while values of ΔH_R are given in units of eV/atom. Data from the literature have been converted to these units using the following values: $1Kj=6.242\times10^{21}$ eV $=239.0$ calories and 1 mole $=N_A=6.022\times10^{23}$.

In Tables I and II we present the heats of reaction calculated as described above for Au and Ag, respectively, on GaAs for various M_rAs_s compound stoichiometries. In Table III we present similar results for Cu on GaAs. For

TABLE I. Heats of reaction of Au with GaAs, including the formation of Au arsenides with various stoichiometries.

Metal arsenide	$\Delta H_f^{\ominus}(M_rAs_s)$ (eV mol^{-1})	$\Delta H_f^{\ominus}(GaM)$ (eV mol^{-1})	$\Delta H_{sol}(Ga;M)$ (eV mol^{-1})	$\Delta H_R^{(3)}$ (eV atom^{-1})	$\Delta H_R^{(4)}$ (eV atom^{-1})	$\Delta H_R^{(5)}$ (eV atom^{-1})
Ga						
GaAs	−0.85[a]					
Au						
AuAs	−0.48[b]	−0.46[c]	−1.00[c]	0.37[d]	−0.09[e]	−0.63[f]
$AuAs_5$	−0.56[b]			3.68[d]	1.38[e]	−1.32[f]
$AuAs_3$	−0.58[b]			1.96[d]	0.58[e]	−1.04[f]
$AuAs_2$	−0.56[b]			1.13[d]	0.21[e]	−0.87[f]
Au_2As	−0.59[b]			0.13[d]	−0.10[e]	−0.37[f]
Au_3As	−0.62[b]			0.07[d]	−0.08[e]	−0.26[f]
Au_5As	−0.62[b]			0.04[d]	−0.05[e]	−0.16[f]
AuAs	−0.48[b]	−0.71[b]	−0.78[b]	0.37[d]	−0.34[e]	−0.41[f]
$AuAs_5$	−0.56[b]			3.68[d]	0.13[e]	−0.22[f]
$AuAs_3$	−0.58[b]			1.96[d]	−0.17[e]	−0.38[f]
$AuAs_2$	−0.56[b]			1.13[d]	−0.29[e]	−0.43[f]
Au_2As	−0.59[b]			0.13[d]	−0.23[e]	−0.26[f]
Au_3As	−0.62[b]			0.07[d]	−0.16[e]	−0.19[f]
Au_5As	−0.62[b]			0.04[d]	−0.10[e]	−0.11[f]

[a]Reference 83.
[b]Reference 68.
[c]Reference 67.
[d]Heat of reaction without alloy formation [Eq. (2)].
[e]Heat of reaction, including formation of the equiatomic alloy GaM [Eq. (3)].
[f]Heat of reaction, including alloying in the dilute limit [Eq. (4)].

TABLE II. Heats of reaction of Ag with GaAs, including the formation of Ag arsenides with various stoichiometries.

Metal arsenide	$\Delta H_f^{\ominus}(M_rAs_s)$ (eV mol^{-1})	$\Delta H_f^{\ominus}(GaM)$ (eV mol^{-1})	$\Delta H_{sol}(Ga;M)$ (eV mol^{-1})	$\Delta H_R^{(3)}$ (eV atom^{-1})	$\Delta H_R^{(4)}$ (eV atom^{-1})	$\Delta H_R^{(5)}$ (eV atom^{-1})
Ga						
GaAs	−0.85[a]					
Ag						
AgAs	−0.31[b]	−0.15[c]	−0.31[c]	0.54[d]	0.39[e]	0.23[f]
$AgAs_5$	−0.37[b]			3.87[d]	3.12[e]	2.32[f]
$AgAs_3$	−0.37[b]			2.17[d]	1.72[e]	1.24[f]
$AgAs_2$	−0.37[b]			1.32[d]	1.02[e]	0.70[f]
Ag_2As	−0.41[b]			0.22[d]	0.15[e]	0.07[f]
Ag_3As	−0.46[b]			0.13[d]	0.08[e]	0.03[f]
Ag_5As	−0.44[b]			0.08[d]	0.05[e]	0.02[f]
AgAs	−0.31[b]	−0.21[b]	−0.22[b]	0.54[d]	0.33[e]	0.32[f]
$AgAs_5$	−0.37[b]			3.87[d]	2.82[e]	2.77[f]
$AgAs_3$	−0.37[b]			2.17[d]	1.54[e]	1.51[f]
$AgAs_2$	−0.37[b]			1.32[d]	0.90[e]	0.88[f]
Ag_2As	−0.41[b]			0.22[d]	0.12[e]	0.11[f]
Ag_3As	−0.46[b]			0.13[d]	0.06[e]	0.06[f]
Ag_5As	−0.44[b]			0.08[d]	0.04[e]	0.04[f]

[a]Reference 83.
[b]Reference 68.
[c]Reference 67.
[d]Heat of reaction without alloy formation [Eq. (2)].
[e]Heat of reaction, including formation of the equiatomic alloy GaM [Eq. (3)].
[f]Heat of reaction, including alloying in the dilute limit [Eq. (4)].

TABLE III. Heats of reaction of Cu with GaAs, including the formation of Cu arsenides with various stoichiometries.

Metal arsenide	$\Delta H_f^{\ominus}(M_rAs_s)$ (eV mol^{-1})	$\Delta H_f^{\ominus}(GaM)$ (eV mol^{-1})	$\Delta H_{sol}(Ga;M)$ (eV mol^{-1})	$\Delta H_R^{(3)}$ (eV atom^{-1})	$\Delta H_R^{(4)}$ (eV atom^{-1})	$\Delta H_R^{(5)}$ (eV atom^{-1})
Ga						
GaAs	−0.85[a]					
Cu						
CuAs	−0.48[b]	−0.21[c]	−0.50[c]	0.37[d]	0.16[e]	−0.13[f]
$CuAs_5$	−0.50[b]			3.74[d]	2.69[e]	1.24[f]
$CuAs_3$	−0.54[b]			2.00[d]	1.37[e]	0.50[f]
$CuAs_2$	−0.53[b]			1.17[d]	0.75[e]	0.17[f]
Cu_2As	−0.69[b]			0.08[d]	−0.02[e]	−0.17[f]
Cu_3As	−0.75[b]			0.03[d]	−0.04[e]	−0.13[f]
Cu_3As	−0.12[g]			0.24[d]	0.17[e]	0.08[f]
Cu_5As	−0.75[b]			0.02[d]	−0.02[e]	−0.08[f]
CuAs	−0.48[b]	−0.25[b]	−0.27[b]	0.37[d]	0.12[e]	0.10[f]
$CuAs_5$	−0.50[b]			3.74[d]	2.49[e]	2.39[f]
$CuAs_3$	−0.54[b]			2.00[d]	1.25[e]	1.19[f]
$CuAs_2$	−0.53[b]			1.17[d]	0.67[e]	0.63[f]
Cu_2As	−0.69[b]			0.08[d]	−0.04[e]	−0.05[f]
Cu_3As	−0.75[b]			0.03[d]	−0.05[e]	−0.06[f]
Cu_3As	−0.12[g]			0.24[d]	0.16[e]	0.15[f]
Cu_5As	−0.75[b]			0.02[d]	−0.03[e]	−0.03[f]

[a]Reference 83.
[b]Reference 68.
[c]Reference 67.
[d]Heat of reaction without alloy formation [Eq. (2)].
[e]Heat of reaction, including formation of the equiatomic alloy GaM [Eq. (3)].
[f]Heat of reaction, including alloying in the dilute limit [Eq. (4)].
[g]Reference 84.

Au we observe that reaction is unfavorable for all compounds if alloying is not included, yet reaction is favorable for all compounds if alloying in the dilute limit is included. For equiatomic alloy formation, reaction is favorable for AuAs and the Au-rich arsenides. We note that the Au-Ga-As ternary phase diagram predicts that $AuGa_2$ is the most stable Au-containing contact to GaAs.[85] In contrast, Ag is not reactive for any of the tabulated compounds in either alloy limit. The results for Cu are similar to those for Au, although, for reactions with alloying; Cu is somewhat less reactive than Au due to the lower heats of formation and solution of Ga in Cu compared to those of Ga in Au. We observe that the most favorable reactions are those which include alloying in the dilute limit. For Au the most favorable reactions are those which include the formation of either $AuAs_2$ or $AuAs_5$. For Cu the most favorable reactions are those for Cu_3As or Cu_2As formation.

We reiterate here the major limitations of these calculations—bulk values for the heats of formation are used (thus neglecting surface energies), thermodynamic equilibrium is assumed (no kinetics or activation energy barriers are accounted for), and only two final phases are considered. However, within these approximations general trends are evident. The extent to which experimental observations of reacted phases differ from those predicted here provides a measure of the importance of these effects.

*Present address: Fairchild Semiconductor Corporation, 4001 Miranda Avenue, Palo Alto, CA 94304.

[1]*Ohmic Contacts to Semiconductors*, edited by B. Schwartz (Electrochemical Society, New York, 1969).
[2]E. H. Rhoderick, *Metal Semiconductor Contacts* (Clarendon, Oxford, 1978).
[3]N. Yokoyama, T. Ohnishi, K. Odani, H. Onodera, and M. Abe, IEEE Trans. Electron Devices **29**, 1541 (1982).
[4]T. Ohnishi, N. Yokoyama, H. Onodera, S. Suzuki, and A. Shibotomi, Appl. Phys. Lett. **43**, 600 (1983).
[5]J. C. Irvin, D. J. Coleman, W. A. Johnson, I. Tatsuguchi, D. R. Kecker, and C. N. Dunn, Proc. IEEE **59**, 1212 (1971).
[6]J. C. Irvin, *Proceedings of the 4th Biennial Cornell Electrical Engineering Conference* (Cornell University Press, Ithaca, N.Y., 1973), pp. 287–298.
[7]G. E. Mahoney, Appl. Phys. Lett. **27**, 613 (1975).
[8]A. K. Sinha and J. M. Poate, Appl. Phys. Lett. **23**, 666 (1973).
[9]A. K. Sinha and J. M. Poate, in *Thin Films—Interdiffusion and Reactions*, edited by J. M. Poate, K. N. Tu, and J. W. Mayer (Wiley-Interscience, New York, 1978), p. 407.
[10]C. J. Madams, D. V. Morgan, and M. J. Howes, Electron. Lett. **11**, 574 (1975).
[11]I. Lindau, P. W. Chye, C. M. Garner, P. Pianetta, C. Y. Su, and W. E. Spicer, J. Vac. Sci. Technol. **15**, 1332 (1978).
[12]W. E. Spicer, I. Lindau, P. Skeath, C. Y. Su, and P. Chye, J Vac. Sci. Technol. **16**, 1422 (1979).

[13]L. J. Brillson, Surf. Sci. Rep. **2**, 123 (1982).
[14]P. W. Chye, I. Lindau, P. Pianetta, C. M. Garner, C. Y. Su, and W. E. Spicer, Phys. Rev. B **18**, 5545 (1978).
[15]L. Brillson, G. Margaritondo, N. G. Stoffel, R. S. Bauer, R. Z. Bachrach, and G. Hansson, J. Vac. Sci. Technol. **17**, 880 (1980).
[16]C. J. Todd, G. W. B. Ashwell, J. D. Speight, and R. Heckingbottom, in *Proceedings of the Conference on Metal-Semiconductor Contacts,* Vol. 22 of *Institute of Physics Conference Series* (IPPS, London, 1974), p. 171.
[17]J. Gyulai, J. W. Mayer, V. Rodriquez, A. Y. C. Yu, and H. J. Gopen, J. Appl. Phys. **42**, 3578 (1971).
[18]G. Y. Robinson, J. Vac. Sci. Technol. **13**, 930 (1976).
[19]Siu Leung, L. K. Wong, D. D. L. Chung, and A. G. Milnes, J. Electrochem. Soc. **130**, 462 (1983).
[20]X.-F. Zeng and D. D. L. Chung, Thin Solid Films **93**, 207 (1982).
[21]K. Kumar, Jpn. J. Appl. Phys. **18**, 713 (1979).
[22]H. K. Kim, G. G. Sweeney, and T. M. S. Heng, in *Proceedings of the 5th International Symposium on GaAs,* Vol. 24 of *Institute of Physics Conference Series* (IPPS, London, 1975), p. 307.
[23]T. Narusawa, N. Watanabe, K. L. I. Kobayashi, and H. Nakashima, J. Vac. Sci. Technol. A **2**, 538 (1984).
[24]E. Kinsbron, P. K. Gallagher, and A. T. English, Solid-State Electron. **22**, 517 (1979).
[25]L. Braicovich, C. M. Garner, P. R. Skeath, C. Y. Su, P. W. Chye, I. Lindau, and W. E. Spicer, Phys. Rev. B **20**, 5131 (1979).
[26]I. Abbati, L. Braicovich, A. Franciosi, I. Lindau, P. Skeath, C. Y. Su, and W. E. Spicer, J. Vac. Sci. Technol. **17**, 930 (1980).
[27]S. Guha, B. M. Arora, and V. P. Salvi, Solid-State Electron. **20**, 431 (1977).
[28]L. Y. Zee and Z. A. Munir, J. Mater. Sci. **10**, 1929 (1975).
[29]D. C. Miller, J. Electrochem. Soc. **127**, 467 (1980).
[30]N. Newman, T. Kendelewicz, D. Thompson, S. H. Pan, S. J. Eglash, and W. E. Spicer, Solid-State Electron. (to be published).
[31]N. Newman, W. G. Petro, T. Kendelewicz, S. H. Pan, S. J. Eglash, and W. E. Spicer, J. Appl. Phys. **57**, 1247 (1985).
[32]P. Pianetta, I. Lindau, and W. E. Spicer, in *ASTM Special Technical Publication 643: Quantitative Surface Analysis of Materials,* edited by N. S. McIntyre (American Society for Testing and Materials, Philadelphia, 1978), p. 105.
[33]K. Yu, Ph.D. thesis, Stanford University, 1976.
[34]J. N. Miller, Ph.D. thesis, Stanford University, 1979.
[35]S. Doniach, I. Lindau, W. E. Spicer, and H. Winick, J. Vac. Sci. Technol. **12**, 1123 (1975).
[36]F. C. Brown, R. Z. Bachrach, and N. Lien, Nucl. Instrum. Methods **152**, 73 (1978).
[37]B. B. Pate, Ph.D. thesis, Stanford University, 1984.
[38]I. Lindau and W. E. Spicer, J. Electron Spectrosc. Rel. Phenom. **3**, 409 (1974).
[39]P. R. Skeath, Ph.D. thesis, Stanford University, 1982.
[40]S.-T. Lee, G. Apai, M. G. Mason, R. Benbow, and Z. Hurych, Phys. Rev. B **23**, 505 (1981).
[41]J. A. Nicholson, J. D. Riley, R. C. G. Leckey, J. G. Jenkin, J. Liesegang, and J. Azoulay, Phys. Rev. B **18**, 2561 (1978).
[42]L. Oberli, R. Monot, H. J. Mathieu, D. Landolt, and J. Buttet, Surf. Sci. **106**, 301 (1981).
[43]A. Zur, T. C. McGill, and D. L. Smith, Phys. Rev. B **28**, 2060 (1983).
[44]R. R. Daniels, A. D. Katnani, T.-X. Zhao, G. Margaritondo, and A. Zunger, Phys. Rev. Lett. **49**, 895 (1982).
[45]D. E. Eastman and W. D. Grobman, Phys. Rev. Lett. **28**, 1327 (1972).
[46]S. Hufner, J. H. Wernick, and K. W. West, Solid State Commun. **10**, 1013 (1972); P. M. T. M. van Attekum, G. K. Wertheim, G. Crecelius, and J. H. Wernick, Phys. Rev. B **22**, 3998 (1980).
[47]I. Lindau, P. Pianetta, K. Y. Yu, and W. E. Spicer, Phys. Rev. B **13**, 492 (1976).
[48]F. R. McFeely, S. Kowalczyk, L. Ley, R. A. Pollack, and D. A. Shirley, Phys. Rev. B **7**, 5228 (1973).
[49]R. E. Watson, J. Hudis, and M. Perlman, Phys. Rev. B **4**, 4139 (1971).
[50]W. F. Egelhoff, Jr. and G. G. Tibbets, Phys. Rev. B **19**, 5028 (1979).
[51]P. Skeath, C. Y. Su, I. Hino, I. Lindau, and W. E. Spicer, Appl. Phys. Lett. **29**, 349 (1981).
[52]D. E. Eastman, T.-C. Chiang, P. Heimann, and F. J. Himpsel, Phys. Rev. Lett. **45**, 656 (1980).
[53]M. K. Bahl, R. O. Woodall, R. L. Watson, and K. J. Irgolic, J. Chem. Phys. **64**, 1210 (1976).
[54]E. D. Roberts, P. Weightman, and C. E. Johnson, J. Phys. C **8**, 1301 (1975).
[55]D. D. Wagman, W. H. Evans, V. B. Parker, I. Halow, S. M. Bailey, and R. H. Schumm, Natl. Bur. Stand. (U.S.) Technical Note 270-S (U.S. GPO, Washington, D.C., 1968).
[56]G. Leonhardt, A. Berndtsson, J. Hedman, M. Klasson, R. Nilsson, and C. Nordling, Phys. Status Solidi **60**, 241 (1973).
[57]M. Taniguchi, S. Suga, M. Seki, H. Sakamoto, H. Kanzaki, Y. Akahama, S. Terada, S. Endo, and S. Narita, Solid State Commun. **45**, 59 (1983).
[58]J. Brunner, M. Thuler, S. Veprek, and R. Wild, J. Phys. Chem. Solids **40**, 967 (1979).
[59]T. Kendelewicz, W. G. Petro, I. Lindau, and W. E. Spicer, J. Vac. Sci. Technol. A **2**, 542 (1984).
[60]P. W. Chye, I. Lindau, P. Pianetta, C. M. Garner, and W. E. Spicer, Phys. Rev. B **17**, 2682 (1978).
[61]T. T. P. Cheung, Surf. Sci. **127**, L129 (1983).
[62]Y. Takasu, R. Unwin, B. Tesche, A. M. Bradshaw, and M. Grunze, Surf. Sci. **77**, 219 (1978).
[63]G. Johansson, J. Hedman, A. Berndtsson, M. Klasson, and R. Nilsson, J. Electron Spectrosc. Rel. Phenom. **2**, 295 (1973).
[64]W. F. Egelhoff, Jr., J. Vac. Sci. Technol. **20**, 668 (1982).
[65]W. F. Egelhoff, Jr., Appl. Surf. Sci. **11/12**, 761 (1982).
[66]T. Kendelewicz (unpublished).
[67]J. F. McGilp, J. Phys. C **17**, 2249 (1984).
[68]A. K. Niessen and A. R. Miedema, Phillips Research Laboratories, Report, 1982 (unpublished).
[69]A. K. Niessen, F. R. de Boer, R. Boom, P. F. de Chatel, W. C. M. Mattens, and A. R. Miedema, CALPHAD: Comput. Coupling Phase Diagrams Thermochem (to be published).
[70]W. E. Spicer, I. Lindau, P. Skeath, C. Y. Su, and P. Chye, Phys. Rev. Lett. **44**, 420 (1980).
[71]W. E. Spicer, I. Lindau, P. Skeath, and C. Y. Su, J. Vac. Sci. Technol. **17**, 1019 (1980).
[72]W. E. Spicer, S. Eglash, I. Lindau, C. Y. Su, and P. Skeath, Thin Solid Films **89**, 447 (1982).
[73]S. H. Pan, T. Kendelewicz, W. G. Petro, M. D. Williams, I. Lindau, and W. E. Spicer, in *Materials Research Society Symposia Proceedings,* Vol. 25 of *Thin Films and Interfaces II,* edited by J. E. E. Baglin, D. R. Campbell, and W. K. Chu (Elsevier, New York, 1984), p. 335.
[74]T. Kendelewicz, W. G. Petro, S. H. Pan, M. D. Williams, I. Lindau, and W. E. Spicer, Appl. Phys Lett. **44**, 113 (1984).
[75]W. E. Spicer, S. Pan, D. Mo, N. Newman, P. Mahowald, T.

Kendelewicz, and S. Eglash, J. Vac. Sci. Technol. B **2**, 476 (1984).

[76]C. J. Cooke and W. Hume-Rothery, J. Less-Common Met. **10**, 42 (1966).

[77]W. Monch, H. J. Clemens, S. Gorlich, R. Enninghorst, and H. Gant, J. Vac. Sci. Technol. **19**, 525 (1981).

[78]J. M. Woodall, G. D. Pettit, T. N. Jackson, C. Lanza, K. L. Kavanaugh, and J. W. Mayer, Phys. Rev. Lett. **51**, 1783 (1983).

[79]T. Kendelewicz, W. G. Petro, M. D. Williams, S. H. Pan, I. Lindau, and W. E. Spicer, in *Materials Research Society Symposia Proccedings,* Vol. 25 of *Thin Films and Interfaces II,* edited by J. E. E. Baglin, D. R. Campbell, and W. K. Chu (Elsevier, New York, 1984), p. 323.

[80]O. Kubaschewski and E. L. Evans, *Metal Physics and Physical Metallurgy* (Pergamon, New York, 1967).

[81]C. H. P. Lupis, *Chemical Thermodynamics of Materials* (North-Holland, New York, 1983).

[82]A. R. Miedema, P. F. de Chatel, and F. R. de Boer, Physica B **100**, 1 (1980).

[83]O. Kubaschewski and C. B. Alcock, *Metallurgical Thermochemistry* (Pergamon, Oxford, 1979).

[84]D. D. Wagman, W. H. Evans, V. B. Parker, R. H. Schumm, I Halow, S. M. Bailey, K. L. Churney, and R. L. Nuttall, J. Phys. Chem. Ref. Data **11**, Suppl. 2, 1 (1982).

[85]R. S. Williams, J. R. Lince, T. C. Tsai, and J. H. Pugh, in *Materials Research Society Symposia Proceedings, 1986* (Materials Research Society, Pittsburgh, Pennsylvania, in press).